A&A 541, L11 (2012)
DOI: 10.1051/0004-6361/201219379

Astronomy & Astrophysics

Letter to the Editor

Detection of the hydroperoxyl radical HO_2 toward ρ Ophiuchi A

Additional constraints on the water chemical network⋆

B. Parise[1], P. Bergman[2], and F. Du[1,⋆⋆]

[1] Max-Planck-Institut für Radioastronomie, Auf dem Hügel 69, 53121 Bonn, Germany
e-mail: bparise@mpifr-bonn.mpg.de
[2] Onsala Space Observatory, Chalmers University of Technology, 43992 Onsala, Sweden

Received 10 April 2012 / Accepted 25 April 2012

ABSTRACT

Context. Hydrogen peroxide (HOOH) was recently detected toward ρ Oph A. Subsequent astrochemical modeling that included reactions in the gas phase and on the surface of dust grains was able to explain the observed abundance, and highlighted the importance of grain chemistry in the formation of HOOH as an intermediate product in water formation. This study also predicted that the hydroperoxyl radical HO_2, the precursor of HOOH, should be detectable.
Aims. We aim at detecting the hydroperoxyl radical HO_2 in ρ Oph A.
Methods. We used the IRAM 30 m and the APEX telescopes to target the brightest HO_2 lines at about 130 and 260 GHz.
Results. We detect five lines of HO_2 (comprising seven individual molecular transitions). The fractional abundance of HO_2 is found to be about 10^{-10}, a value similar to the abundance of HOOH. This observational result is consistent with the prediction of the above mentioned astrochemical model, and thereby validates our current understanding of the water formation on dust grains.
Conclusions. This detection, anticipated by a sophisticated gas-grain chemical model, demonstrates that models of grain chemistry have improved tremendously and that grain surface reactions now form a crucial part of the overall astrochemical network.

Key words. astrochemistry – line: identification – ISM: abundances – ISM: molecules – ISM: individual objects: ρ Ophiuchi A

1. Introduction

Water is an essential molecule in star-forming regions, in particular because it is the main constituent of the icy mantles of dust grains, one of the main repositories of oxygen, and in certain conditions an important gas coolant (e.g. Nisini et al. 2010). It is moreover detected in virtually all star-forming environments in which it is searched for (e.g. Caselli et al. 2010; Hogerheijde et al. 2011; van Dishoeck et al. 2011).

Water is believed to form efficiently on the surface of dust grains through several different pathways. The relative importance of these pathways is not completely understood, however, and the reaction barriers involved are still under debate despite numerous recent laboratory experiments (Ioppolo et al. 2010; Cuppen et al. 2010). This is because isolating a particular reaction in the laboratory is extremely difficult, and the absolute measure of the reaction rates and barriers on the grains is almost impossible.

In this sense, astronomical observations of the precursors of water can be of great help to constrain the chemical network that leads to water formation. A significant step in the understanding of water formation was achieved thanks to the detection with APEX of HOOH in Oph A (Bergman et al. 2011b). This detection has been carefully modeled with an astrochemical model combining reactions in the gas phase and on the grain surfaces based on the hybrid moment equation (HME) method (Du & Parise 2011), applied to the conditions of the Oph A cloud (Du et al. 2012). The model successfully reproduces simultaneously the abundances of the observed gas-phase HOOH, O_2, H_2CO and CH_3OH. The model also predicts that the hydroperoxyl radical (HO_2, or O_2H), the direct precursor leading to HOOH via hydrogenation, has a significant abundance, which makes its detection with current radio telescopes possible. Hydroperoxyl has not yet – to our knowledge – been detected in the interstellar medium in either its solid or its gaseous form.

We aim here at detecting this radical toward the SM1 core of the ρ Oph A cloud, where HOOH and O_2 (Liseau et al. 2012) were detected. The paper is organized as follows. The observations are presented in Sect. 2, and the results in Sect. 3. We discuss the implications of this detection in Sect. 4.

2. Observations

The HO_2 radical is a light asymmetric rotor with an unpaired electronic spin. This causes each asymmetric rotor level (except $0_{0,0}$) to be split into a doublet of states. This is illustrated in the HO_2 energy level diagram in Fig. 1 where all states below 50 K are shown. It is based on the JPL catalog (Pickett et al. 1998), which uses mm and submm spectroscopy data from Beers & Howard (1975), Saito (1977), and Charo & de Lucia (1982). Also, the hyperfine splitting is large enough to be detectable. The spectrum of HO_2 exhibits both a- and b-type transitions with associated dipole moments $\mu_a = 1.41$ D and $\mu_b = 1.54$ D (Saito & Matsumura 1980).

⋆ Based on observations carried out with the IRAM 30 m and the APEX telescopes. IRAM is supported by INSU/CNRS (France), MPG (Germany) and IGN (Spain). APEX is a collaboration between the Max Planck Institute for Radio Astronomy, the Onsala Space Observatory, and the European Southern Observatory.

⋆⋆ Member of the International Max Planck Research School (IMPRS) for Astronomy and Astrophysics at the Universities of Bonn and Cologne.

Table 1. The HO_2 and SO_2 lines detected in the same setups.

Line	Frequency (GHz)	Quantum numbers Rotation	$J_u \rightarrow J_l$	$F_u \rightarrow F_l$	A_{ul} (s^{-1})	E_u (K)	g_u	$\int T_{mb} dv$ (mK s^{-1})	Δv (km s^{-1})	v_{lsr} (km s^{-1})
1	130.26007	$2_{0,2} \rightarrow 1_{0,1}$	5/2 → 3/2	3 → 2	2.07×10^{-5}	9.4	7	74 ± 7	0.66 ± 0.07	4.6 ± 0.1
2	130.25813	$2_{0,2} \rightarrow 1_{0,1}$	5/2 → 3/2	2 → 1	1.85×10^{-5}	9.4	5	54 ± 8	0.65 ± 0.11	4.6 ± 0.1
3	130.46741	$2_{0,2} \rightarrow 1_{0,1}$	3/2 → 1/2	2 → 1	1.76×10^{-5}	9.4	5	45 ± 4	0.54 ± 0.06	3.0 ± 0.1
	130.46368	$2_{0,2} \rightarrow 1_{0,1}$	3/2 → 1/2	1 → 0	1.16×10^{-5}	9.4	3	<26		
4a	260.56614	$4_{0,4} \rightarrow 3_{0,3}$	9/2 → 7/2	5 → 4	1.86×10^{-4}	31.3	11	} 115 ± 14	} 0.88 ± 0.13	–
4b	260.56566	$4_{0,4} \rightarrow 3_{0,3}$	9/2 → 7/2	4 → 3	1.81×10^{-4}	31.3	9			
5a	260.77030	$4_{0,4} \rightarrow 3_{0,3}$	7/2 → 5/2	4 → 3	1.80×10^{-4}	31.3	9	} 61 ± 13	} 0.91 ± 0.24	–
5b	260.76967	$4_{0,4} \rightarrow 3_{0,3}$	7/2 → 5/2	3 → 2	1.72×10^{-4}	31.3	7			
SO_2	129.51481	$10_{2,8} \rightarrow 10_{1,9}$						199 ± 6	0.64 ± 0.02	3.8 ± 0.1
SO_2	131.01486	$12_{1,11} \rightarrow 12_{0,12}$						168 ± 5	0.68 ± 0.03	3.7 ± 0.1

Notes. For lines 1 to 3 and SO_2, the frequencies are those measured in the laboratory and tabulated in the JPL database. The v_{lsr} of the lines are therefore computed based on these frequencies. The hyperfine structure frequencies of lines 4 and 5 were computed from the energies tabulated in the JPL database (http://spec.jpl.nasa.gov/ftp/pub/catalog/archive/c033001.egy). Uncertainties on fluxes, linewidths and v_{lsr} are 1σ. The upper limit on the $F = 1 \rightarrow 0$ line is the flux of the bump at the expected frequency (see Fig. 2).

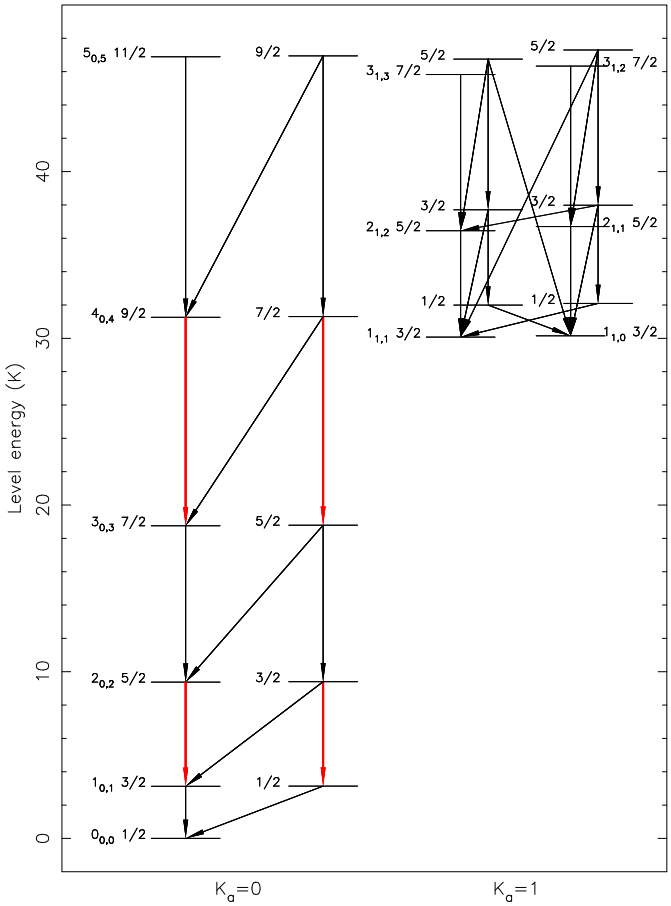

Fig. 1. Energy level diagram of HO_2 below 50 K. Only the *a*-type transitions listed in the JPL catalog were included and are drawn as arrows. Red arrows indicate observed transitions. The *b*-type transitions (connecting $K_a = 0$ and 1 states) were omitted for the sake of clarity. Next to each level the quantum number designation is listed.

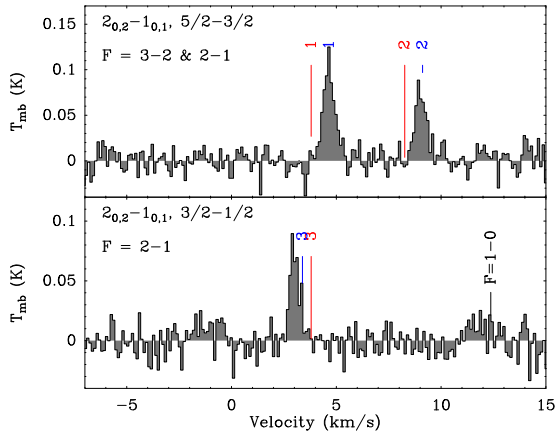

Fig. 2. Lines observed with the IRAM telescope. The red bars show the expected frequencies for the different lines, as measured in the laboratory (Saito 1977). The blue bars show the calculated frequencies from Charo & de Lucia (1982). The black vertical line in the lower panel shows the position of the undetected $F = 1 \rightarrow 0$ line.

We targeted lines of the HO_2 radical at 130.3 GHz and 260.6 GHz (see Table 1), which were observed in the laboratory by Saito (1977) and Charo & de Lucia (1982), respectively. We used the frequencies tabulated in the JPL database, which correspond to the measured values for these lines. The $1_{0,1} \rightarrow 0_{0,0}$ lines around 65 GHz are poorly suited for a ground-based search because they are heavily affected by the strong atmospheric absorption due to O_2. The $3_{0,3} \rightarrow 2_{0,2}$ lines (at 195 GHz) fall in a frequency region where few receivers are currently in operation. They are also somewhat affected by the atmospheric absorption from the 183 GHz water line. Likewise, the $5_{0,5} \rightarrow 4_{0,4}$ lines are affected by the atmospheric 325 GHz water line. Hence, the targeted lines at 130 and 260 GHz are the best candidates for a detection in a low-excitation source (for which most of the population is likely to reside in the lower $K_a = 0$ levels).

All observations targeted the SM1 position at $\alpha(2000) = 16^h26^m27\overset{s}{.}20$, $\delta(2000) = -24°24'04''$. The IRAM 30 m observations were carried out on Dec. 5, 2011, under average weather conditions with a precipitable water vapour (PWV) column of 5 mm. The EMIR receiver (Carter et al. 2012) was tuned in both polarizations to 130.3 GHz. The angular resolution of the observations is 19″ at this frequency. The receiver was connected to FTS spectrometers, which were used in their highest resolution mode, providing a 50 kHz resolution. The focus was optimized on Saturn at the beginning of the observations. The pointing was checked locally every hour, either on 1741-038, 1622-297,

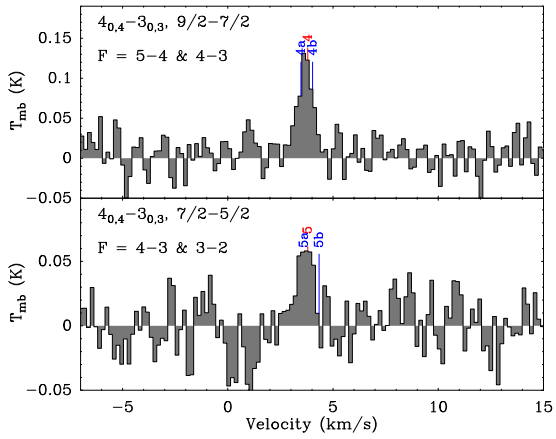

Fig. 3. Lines observed with the APEX telescope. The data were smoothed to a resolution of 0.18 km s^{-1}. The red bars show the expected frequencies for the different lines, as measured in the laboratory (Charo & de Lucia 1982). The blue bars show the computed hyperfine frequencies (see Table 1).

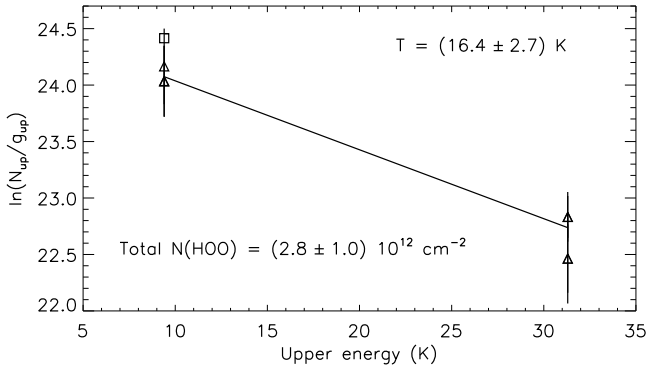

Fig. 4. HO_2 rotational diagram. A source size of 24″ is assumed. The triangles correspond to detected lines. The square corresponds to the upper limit of the flux on the undetected line at 130.464 GHz.

or 1730-130, depending on the time of the pointing, and was found to be better than 3.″8 (rms). For the conversion to the T_{mb} scale, we adopt a main beam efficiency of 0.76, as extrapolated from the values given on the IRAM website[1].

The APEX observations were carried out on Oct. 10 and 16, 2011, under variable weather conditions (PWV = 2.3–3.7 mm on Oct. 10, PWV = 0.6 mm on Oct. 16). The APEX1 receiver (Vassilev et al. 2008) was tuned to 260.25 GHz and connected to the XFFTS backend, leading to a velocity resolution of 0.09 km s^{-1}. The angular resolution of the observations at this frequency is 24″. Because no planet was available during the observations, the focus was optimized on IRAS 15194-5115 by maximizing the CO(2–1) line flux. The pointing was checked every hour by observing CO(2–1) on RAFGL1922, and was found to be always better than 3″.

3. Results

Figure 2 displays the three lines targeted with the IRAM telescope, and Fig. 3 shows the two lines targeted with APEX. Over the wide bandwidth observed with the FTS, no obvious other line is present, except for two SO_2 lines, which allow us to confirm the v_{lsr} (3.8 km s^{-1}) and line width of the expected lines (see Table 1).

We detected three HO_2 lines with the IRAM telescope with a high signal-to-noise ratio, whose linewidths are consistent with the linewidth measured for the SO_2 lines, but whose frequencies do not coincide exactly with those measured in the laboratory by Saito (1977), shown as red vertical bars in Fig. 2 (assuming a v_{lsr} of 3.8 km s^{-1}). Saito (1977) estimated an uncertainty on the laboratory frequency of 0.2 MHz (i.e. 0.5 km s^{-1} at 130 GHz). Charo & de Lucia (1982) measured the frequency of other lines between 150 and 550 GHz, and used the full dataset available at that time (including Saito's lines) to fit the HO_2 Hamiltonian. They found in particular a significant discrepancy (0.37 MHz) between the frequency measured by Saito (1977) and the calculated frequency from the Hamiltonian for the two lines at 130.26 GHz, which they excluded from their fit. The blue bars in Fig. 2 show the calculated frequency from Charo & de Lucia (1982). The first two detected lines coincide very closely with their theoretical frequencies. When adopting these new frequency values, the v_{lsr} of the lines become 3.8 and 3.7 km s^{-1}, respectively, which is fully consistent with the source velocity as determined by SO_2 and several other molecules in the SM1 source (Bergman et al. 2011a). The third line is still slightly offset, with a v_{lsr} of 3.4 km s^{-1}.

Because the source is relatively line-poor, we can assign the three lines to HO_2 with a high confidence level. An additional line (at 130.46368 GHz) is only tentatively detected, and we consider in the following only an upper limit on its flux. No blend with other plausible molecules was found at these frequencies in either the CDMS (Müller et al. 2001) or the JPL catalog (Pickett et al. 1998).

We detected two additional lines of HO_2 with the APEX telescope. Both lines have an unresolved hyperfine structure. A Gaussian fit of these two lines leads to a broader line width than for the other lines (see Table 1), but this may be because of the hyperfine splitting, which for these lines corresponds to about 0.6–0.7 km s^{-1}. Here again, no blend with any other plausible molecule is found.

In summary, we report here the detection of five different spectral features assigned to seven different lines of HO_2.

4. Analysis and discussion

We use the rotation diagram method to derive the abundance of HO_2, which assumes that the population distribution can be described by a single temperature, and that lines are optically thin. The rotation diagram obtained with the five detected spectral features is presented in Fig. 4. We assume for lines 4 and 5 that the measured flux is coming from the two unresolved hyperfine components proportionally to $A_{ul} \times g_u$, as expected for two optically thin lines originating from two levels of the same energy. We assume a source size of 24″, as for hydrogen peroxide (Bergman et al. 2011b), and as derived by the analysis of Bergman et al. (2011a). We derive a rotational temperature of 16 ± 3 K, slightly lower than the rotational temperature derived for HOOH (22 ± 3 K, Bergman et al. 2011b), but marginally consistent with it within the error bars. The derived HO_2 column density is $(2.8 \pm 1.0) \times 10^{12}$ cm^{-2}. This column density results in optically thin lines. Forcing the rotational temperature to be 22 K as for HOOH, we derive a column density for HO_2 of 3.0×10^{12} cm^{-2}, very close to the column density derived with the fitted T_{rot} of 16.4 K.

The relatively high A_{ul} of the 260 GHz lines (and the even higher spontaneous rates of the *b*-type transitions) indicate that

[1] http://www.iram.es/IRAMES/mainWiki/Iram30mEfficiencies

the excitation could be somewhat subthermal for the density in SM1 (10^5–10^6 cm^{-3}, Bergman et al. 2011a). This could imply that our derived column density is too high. To estimate this, we simply truncate the partition function such that the summation only takes place over $K_a = 0$ states below 40 K and compare the result to the full partition function. We then find that the truncated part holds about 70% of the level populations at $T = 16$ K. Therefore, in the unlikely case of extreme subthermal excitation (no population in $K_a > 0$ states and in $K_a = 0$ states above $4_{0,4}$), we may explain the observations by adopting a 30% lower HO_2 column density. This lower column density falls within the errors and we conclude that subthermal excitation will have a minor impact on our derived column density.

From the H_2CO and CH_3OH analysis of the SM1 core, Bergman et al. (2011a) determined an H_2 column density of 3×10^{22} cm^{-2}. The abundance of HO_2 is therefore $\sim 10^{-10}$.

The gas-grain chemical model of Du et al. (2012), based on the detection of HOOH and other molecules, predicts that the HO_2/HOOH abundance ratio in ρ Oph A should be about three. In this model, at $T \sim 20$ K, HO_2 is mainly formed on dust grains through the barrierless reaction O + OH at an early stage ($<5 \times 10^4$ yr), and through the reaction H + O_2 at a later stage. Here, we find observationally HO_2/HOOH ~ 1, which is consistent with the model, taking into account the excitation uncertainty. This result is therefore an additional validation of our understanding of water formation on dust grains.

Motivated by our detection, we inspected previous spectral surveys for unidentified lines at the frequencies of the HO_2 molecule. No line is detected in the TIMASSS survey (Caux et al. 2011) toward the low-mass protostar IRAS 16293−2422. Nummelin et al. (1998) reported (in their Table 46) two unidentified lines in their Sgr B2 survey that might correspond to HO_2 frequencies, U260568 and U260771 toward Sgr B2(N) and U260569 toward Sgr B2(M). Because the lines have typical widths of 13 km s^{-1}, line blending is a severe limiting factor for a secure line assignment. The Sgr B2 IRAM 30 m line survey coverage does not include the lines at 130 GHz (Belloche, priv. comm.). A 2 mm unpublished survey from B. Turner made with the NRAO 12 m telescope between 1993 and 1995 covers the two 130.26 GHz lines (but not the 130.46 GHz lines, Remijan et al. 2008). This doublet unfortunately falls very close to the $J = 3$–2 SiO emission/absorption feature at 130 268.7 MHz, making it very difficult to discern any weaker HO_2 lines. Assuming that the unidentified lines of the Sgr B2(N) survey by Nummelin et al. (1998) are assigned to HO_2, and assuming $T_{\rm rot} = 50$ K (Nummelin et al. 2000), we find $N(HO_2) \leq 1.1 \times 10^{14}$ cm^{-2}, averaged in the 20″ beam. Using the H_2 column density derived by Nummelin et al. (3×10^{24} cm^{-2}), this results in an upper limit on the fractional abundance of HO_2 of 4×10^{-11}, somewhat below the detected abundance toward ρ Oph A.

The result of this work is one of the rare examples of the detection of a new molecule after it was predicted by chemical modeling (Du et al. 2012). Other examples include the detection of CF^+ (Neufeld et al. 2006), motivated also by (gas-phase) model predictions. The novelty here is that the detection of HO_2 was predicted by models describing the chemistry on dust grain surfaces. This shows the increasing predictive power of these models, thanks to the numerical refinements developed to correctly treat the stochasticity of surface chemistry (e.g. Garrod et al. 2009; Du & Parise 2011), and the recent numerous laboratory experiments (e.g. Oba et al. 2009; Ioppolo et al. 2010; Cuppen et al. 2010). The era when dust chemistry could be described as "the last refuge of the scoundrels" (Charnley et al. 1992) seems to be over.

Acknowledgements. We thank the referee, P. Goldsmith, for comments that helped improving the manuscript. We are grateful to the IRAM director, P. Cox, for granting us directorial time on the IRAM 30 m telescope. We thank A. Gusdorf for carrying out the APEX observations. B.P. and F.D. are supported by the German Deutsche Forschungsgemeinschaft, DFG Emmy Noether project number PA1692/1-1.

References

Beers, Y., & Howard, C. J. 1975, J. Chem. Phys., 63, 4212
Bergman, P., Parise, B., Liseau, R., & Larsson, B. 2011a, A&A, 527, A39
Bergman, P., Parise, B., Liseau, R., et al. 2011b, A&A, 531, L8
Carter, M., Lazareff, B., Maier, D., et al. 2012, A&A, 538, A89
Caselli, P., Keto, E., Pagani, L., et al. 2010, A&A, 521, L29
Caux, E., Kahane, C., Castets, A., et al. 2011, A&A, 532, A23
Charnley, S. B., Tielens, A. G. G. M., & Millar, T. J. 1992, ApJ, 399, L71
Charo, A., & de Lucia, F. C. 1982, J. Mol. Spect., 94, 426
Cuppen, H. M., Ioppolo, S., Romanzin, C., & Linnartz, H. 2010, Phys. Chem. Chem. Phys. (Incorporating Faraday Transactions), 12, 12077
Du, F., & Parise, B. 2011, A&A, 530, A131
Du, F., Parise, B., & Bergman, P. 2012, A&A, 538, A91
Garrod, R. T., Vasyunin, A. I., Semenov, D. A., Wiebe, D. S., & Henning, T. 2009, ApJ, 700, L43
Hogerheijde, M. R., Bergin, E. A., Brinch, C., et al. 2011, Science, 334, 338
Ioppolo, S., Cuppen, H. M., Romanzin, C., van Dishoeck, E. F., & Linnartz, H. 2010, Phys. Chem. Chem. Phys. (Incorporating Faraday Transactions), 12, 12065
Liseau, R., Goldsmith, P. F., Larsson, B., et al. 2012, A&A, 541, A73
Müller, H. S. P., Thorwirth, S., Roth, D. A., & Winnewisser, G. 2001, A&A, 370, L49
Neufeld, D. A., Schilke, P., Menten, K. M., et al. 2006, A&A, 454, L37
Nisini, B., Benedettini, M., Codella, C., et al. 2010, A&A, 518, L120
Nummelin, A., Bergman, P., Hjalmarson, Å., et al. 1998, ApJS, 117, 427
Nummelin, A., Bergman, P., Hjalmarson, Å., et al. 2000, ApJS, 128, 213
Oba, Y., Miyauchi, N., Hidaka, H., et al. 2009, ApJ, 701, 464
Pickett, H. M., Poynter, R. L., Cohen, E. A., et al. 1998, J. Quant. Spec. Radiat. Transf., 60, 883
Remijan, A. J., Leigh, D. P., Markwick-Kemper, A. J., & Turner, B. E. 2008 [arXiv:0802.2273]
Saito, S. 1977, J. Mol. Spect., 65, 229
Saito, S., & Matsumura, C. 1980, J. Mol. Spect., 80, 34
van Dishoeck, E. F., Kristensen, L. E., Benz, A. O., et al. 2011, PASP, 123, 138
Vassilev, V., Meledin, D., Lapkin, I., et al. 2008, A&A, 490, 1157